Energetics and structural relaxation of constitutional defects in CoAl and CoTi from first principles

Masataka Mizuno,* Hideki Araki, and Yasuharu Shirai
Science and Technology Center for Atoms, Molecules and Ions Control, Graduate School of Engineering, Osaka University, 2-1 Yamadaoka, Suita 561-0874, Japan
(Received 1 May 2003; published 7 October 2003)

The energetics and structural relaxations of constitutional defects in CoAl and CoTi are investigated using first-principles electronic structure calculations. In order to estimate the stability of the constitutional defects, the compositional dependence curves of the formation energy are obtained from the calculations employing supercells of various sizes. The difference in the bonding character induces the difference in the energetics and structural relaxations of the defects between CoAl and CoTi: A covalent bonding character is more pronounced in CoAl than in CoTi and CoTi has a larger ionic bonding character than CoAl. The Co vacancy is energetically more favorable than the Al antisite in Al-rich CoAl, whereas the opposite trend is observed in Ti-rich CoTi. The Ti-*d* orbital at the antisite and the excess electrons play an important role for the stability of the Ti antisite atom. The relaxation around the constitutional defects in CoAl and CoTi cannot be explained by only the atomic size difference. The change in the bonding charge density as a result of the charge redistribution around the defects plays a key role in the structural relaxation. This situation originates from the mixture of the ionic and covalent bonding character in intermetallic compounds. The ionic bonding character leads to the effective charge around the defects and the covalent bonding is affected by the charge redistribution screening the effective charge. The ionic bonding character in CoTi brings about the outward relaxations of the neighboring atoms around the Co antisite atom and the Ti vacancy in CoTi.

DOI: 10.1103/PhysRevB.68.144103 PACS number(s): 61.72.Ji, 61.72.Bb, 71.20.Lp

I. INTRODUCTION

The transition-metal (TM) aluminides and titanides have attracted considerable attention due to their physical and mechanical properties. These intermetallic compounds exist in a wide range of concentration around the stoichiometry. In order to compensate the deviation from the stoichiometry, constitutional defects are introduced. Experimental and theoretical studies have been performed for the constitutional defects because several properties, such as mechanical and magnetic properties, show compositional dependence originating from the structural defects.

The effective formation energies of vacancies and antisite atoms on both sublattices have been calculated by a combination of *ab initio* electron theory and statistical mechanics for NiAl and FeAl by Fu *et al.*,[1] FeAl by Mayer *et al.*,[2] CoAl by Bester *et al.*,[3] and NiAl by Meyer *et al.*[4] They mainly discussed the dominant thermal excitations by comparison with experimental results, whereas the electronic structure of these defects was not focused. The electronic structures of the vacancies and antisite atoms for FeAl, CoAl, and NiAl have been calculated using the tight-binding linear muffin-tin orbital method for discussing the magnetic moment around the defects in detail.[5] Earlier theoretical calculations for defects in CoAl and CoGa reveal that the electronic structure of the Co antisite atom in CoAl is strongly influenced by the nearest-neighbor Co atoms and differs from that of the Co atom in bulk CoAl.[6] Origin of defects was discussed for PdAl, FeAl, and NiAl systems using the density-of-states profile of the bulk systems obtained by first-principles calculations.[7] It was shown that the size effect is inadequate in explaining the defect structure in these intermetallics, and the electronic structure at the transition-metal sites is most important in determining the energetics of defects. Börnsen *et al.* studied the change in the bonding property by the formation of the defects for FeAl, CoAl, and NiAl.[8] They reported that for the case of B2 aluminides the defect energetics cannot be traced back to the properties of the TM-*d*–Al-*sp* bonds and are determined by the net effect of many competing energetic contributions of comparable size. On the other hand, although the electronic structure of B2 titanides has been studied by several authors,[9–11] little attention has been given to defects in B2 titanides.

From experimental point of view, one of the most powerful tools for the investigation of lattice defects is positron annihilation spectroscopy. The combination of experimental positron lifetimes and its theoretical calculations allows us to characterize vacancy-type defects. For the accurate characterization, it is important to take the structural relaxation around vacancies into account in the positron lifetime calculation, because the positron lifetime is inversely proportional to the electron density where the positron is annihilated. The inward relaxation around a vacancy trapping a positron decreases the positron lifetime, and the outward relaxation has the opposite effect.[12] However, there are few theoretical works that refer to the structural relaxation in intermetallic compounds. It may be unreliable to speculate the structural relaxation by the atomic size difference because the size effect is not always responsible for the energetics of defects.

In this paper, we consider monovacancies and antisite atoms as constitutional defects in CoAl and CoTi. We have performed first-principles electronic structure calculations in order to investigate the energetics and structural relaxation of the defects. While the atomic radii of Al and Ti are comparable, the bonding character of the Co-Al bonds in CoAl and

TABLE I. The supercell size and chemical composition including a constitutional defect.

Defect	Supercell	N	Number of atoms	Composition (at. % Ti/Al)
(Al/Ti) Vacancy	$2\times2\times2$	16	Co 8, (Ti/Al) 7	46.67
	$3\times3\times3$	54	Co 27, (Ti/Al) 26	49.06
	$4\times4\times4$	128	Co 64, (Ti/Al) 63	49.61
Co vacancy	$2\times2\times2$	16	Co 7, (Ti/Al) 8	53.33
	$3\times3\times3$	54	Co 26, (Ti/Al) 27	50.94
	$4\times4\times4$	128	Co 63, (Ti/Al) 64	50.39
(Al/Ti) antisite	$2\times2\times2$	16	Co 7, (Ti/Al) 9	56.25
	$3\times3\times3$	54	Co 26, (Ti/Al) 28	51.85
	$4\times4\times4$	128	Co 63, (Ti/Al) 65	50.78
Co antisite	$2\times2\times2$	16	Co 9, (Ti/Al) 7	43.75
	$3\times3\times3$	54	Co 28, (Ti/Al) 26	48.15
	$4\times4\times4$	128	Co 65, (Ti/Al) 63	49.22

the Co-Ti bonds in CoTi will be different. Comparing aluminides and titanides, therefore, can provide clues to understanding the role of the electronic structure and the atomic size difference for not only the defect energetics but also the structural relaxation around defects. The paper is organized as follows. The calculation method is described in Sec. II. The formation energies of CoAl and CoTi including the constitutional defects and the structural relaxations are presented in Sec. III. We discuss the electronic structure of the monovacancy and the antisite atoms using the density of states and charge-density maps in Sec. IV. The conclusions of this work are summarized in Sec. V.

II. CALCULATION DETAILS

In order to obtain the electronic structures for the constitutional defects, we employed a first-principles plane-wave pseudopotential code VASP (Vienna *ab initio* simulation package)[13–16] with generalized gradient approximation proposed by Perdew and Wang.[17]

First, we calculated the equilibrium lattice constant using the kinetic-energy cutoff of 350 eV and a $16\times16\times16$ k mesh in the Monkhorst-Pack scheme with the unit cell including two atoms. The Ti-3p electrons were treated as valence electrons. We obtained the equilibrium lattice constant of 2.855 Å for CoAl and 2.982 Å for CoTi, which reproduces the experimental values within 1%. We estimate the stability of the constitutional defects by the formation energies of CoAl and CoTi including the constitutional defects. The formation energies were calculated by subtracting the total energy of constituent elemental solids from the total energy of the compounds. One of the difficulties for the comparison of the stability of the constitutional defects is that supercell models having the same chemical composition cannot be constructed. In the case of the $3\times3\times3$ models for CoAl, the Al composition of the Al vacancy model is 49.06 at. % whereas that of the Co antisite model is 48.15 at. %. In order to compare the formation energies with various chemical compositions, the formation energies of supercell models in various sizes ($2\times2\times2$, $3\times3\times3$, and $4\times4\times4$) were calculated and we obtained the composition dependence curves of the formation energies. The total numbers of the lattice site, N, in the $2\times2\times2$, $3\times3\times3$, and $4\times4\times4$ supercells are 16, 54, and 128, respectively. For the defect calculations, relaxations of the atomic positions were allowed and the volume of the supercell was fixed.The chemical composition and supercell size are listed in Table I.

Table II shows the k-mesh size dependence of the formation energy and the lattice relaxation for the $N=54$ supercell model for the Co vacancy in CoTi. A $4\times4\times4$ k mesh is sufficient to guarantee the formation energy of 0.01 eV per atom, whereas a $6\times6\times6$ k mesh is required for the lattice relaxation. The calculations of the $N=16$ and 54 supercell models were, therefore, done using a $6\times6\times6$ k mesh. For the $N=128$ supercell models, the $4\times4\times4$ k mesh was employed because of the limitation of the computer resources. It is noted that the $4\times4\times4$ k mesh for the $N=128$ supercell models guarantees sufficient convergence for the formation energy but the lattice relaxations are not well converged. We discuss the relaxed structures around the defects using the results of the $N=54$ supercell models with the $6\times6\times6$ k mesh. The structural relaxation was performed until forces on all atoms become less than 0.01 eV/Å, which also converges the total energy within 1 meV.

The ordered stoichiometric CoAl and CoTi are nonmagnetic, but there can be a magnetic moment in those of nonstoichiometric ones.[18,19] Stefanou *et al.* performed first-principles calculations for point defects in CoAl and CoGa and found that the Co antisite atom is magnetic.[6] In order to estimate the influence of spin polarization on the formation energy and the lattice relaxation, spin-polarized calculations

TABLE II. The formation energies of the $N=54$ supercell model for the Co vacancy in CoTi and the lattice relaxations of the neighboring Ti atoms around the Co vacancy.

k mesh	Formation energy (eV/atom)	Relaxation (%)
$2\times2\times2$	-7.765	-2.374
$4\times4\times4$	-7.776	-1.874
$6\times6\times6$	-7.774	-1.978
$8\times8\times8$	-7.774	-1.978

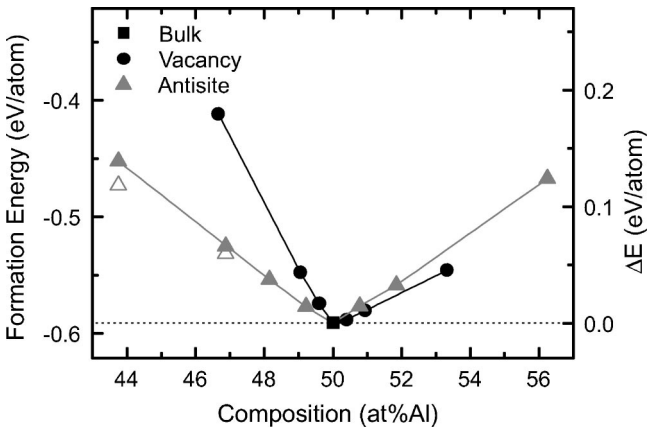

FIG. 1. The formation energy of CoAl including a constitutional defect as a function of Al composition. Open marks represent the results by the spin-polarized calculations.

were also performed for the supercells including the Al/Ti vacancy as well as the Co antisite atom because the Co-Co interaction around the Al/Ti vacancy could be enhanced by the charge redistribution or structural relaxation. The spin-polarized calculations using the $N=128$ supercell models were omitted due to the limitation of the computer resources.

III. ENERGETICS AND STRUCTURAL RELAXATIONS FOR CONSTITUTIONAL DEFECTS

Figures 1 and 2 show the formation energies as a function of the Al composition in CoAl and the Ti composition in CoTi, respectively. Additional calculation with the $N=32$ supercell was performed only for the Co antisite atom in CoAl in order to examine the composition dependence of spin polarizations. In CoTi, the antisite defect is more stable than the vacancy in all the regions. On the other hand, in the Al-rich CoAl, the Co vacancy is slightly more stable than the Al antisite defect. The minimum of the formation energy for the Co antisite in CoTi is shifted from the stoichiometry toward the Co-rich side by about 1 at. %. These results for CoAl correspond to the effective formation energies of vacancies

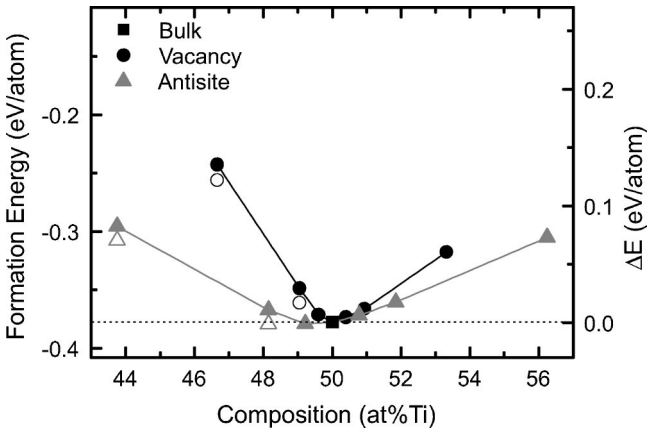

FIG. 2. The formation energy of CoTi including a constitutional defect as a function of Ti composition. Open marks represent the results by the spin-polarized calculations.

TABLE III. The lattice relaxations of the first and second nearest-neighbor atoms around a constitutional defect in CoAl and CoTi calculated with the $N=54$ supercell, given as a percentage of the nearest-neighbor (NN) bond length in bulk CoAl and CoTi.

	Defect	Relaxation (%)	
		First NN	Second NN
CoTi			
	Co vacancy	−1.978	1.752
	Ti vacancy	7.241	−6.300
	Spin polarized	1.916	−4.056
	Co antisite	6.347	−8.156
	Spin polarized	3.824	−5.743
	Ti antisite	1.756	1.873
CoAl			
	Co vacancy	−3.215	1.308
	Al vacancy	−0.719	−1.710
	Co antisite	−0.197	−1.485
	Al antisite	3.777	−1.837

and antisite atoms in CoAl calculated by a combination of *ab initio* electron theory and statistical mechanics.[3] For CoTi, the stability of the Co antisite atoms in the Co-rich side agrees with the positron annihilation measurement, indicating that antisite atoms are responsible for the deviation from the stoichiometry in the Co-rich side.[20] For the Co-rich side in CoTi, the positron annihilation measurement suggests that constitutional vacancies are introduced at 50.5 at. % Ti that is close to the compositional limit in the Ti-rich side of the B2 structure. However, it seems to be difficult to further discuss the constitutional defects in the Ti-rich side because of the narrow compositional range in the Ti-rich side.

In Co-rich CoTi, the formation energies obtained from the spin-polarized calculations are lower than from the non-spin-polarized calculations. The energy differences between non-spin- and spin-polarized calculations are not too large to change the priority of the Co antisite atoms in the Co-rich side, but the formation energy at 48.15 at. % Ti including the Co antisite becomes lower than that at stoichiometric composition as a result of the spin-polarized calculation. On the other hand, only the Co antisite atom becomes more stable in Co-rich CoAl. This is because the Al vacancy in CoAl does not show a significant spin split. In addition, the dependence of the spin polarization on the supercell size appears for the Co antisite atoms in CoAl: The energy gain decreases linearly with the supercell size and the $N=54$ supercell calculation does not yield a clear spin split. The origin of the dependence will be discussed later.

The structural relaxations around the constitutional defects calculated using the $N=54$ supercell are listed in Table III. The larger structural relaxation around a defect at the Al/Ti site is expected than that at the Co site because the atomic radius of Ti and Al is about 15% larger than that of Co. This speculation is almost applicable for the case of CoAl except that the relaxation around the Co vacancy is larger than that around the Al vacancy. The similar tendency was reported for the case of NiAl.[4] On the other hand, the relaxation around the Ti vacancy and Co antisite in CoTi

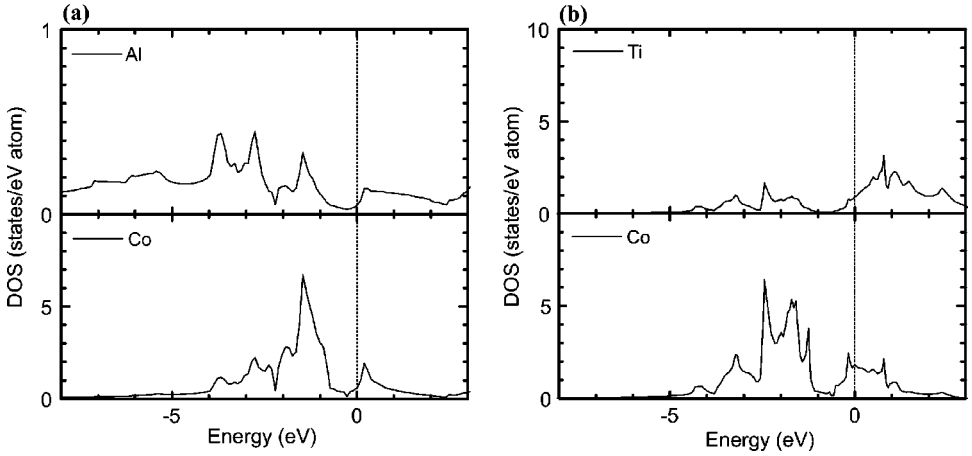

FIG. 3. The site-projected PDOS for the bulk systems of (a) CoAl and (b) CoTi.

shows large outward displacement in spite of the inward relaxation expected from the atomic size difference. The spin-polarized calculations for Ti vacancy and Co antisite in CoTi reduce the magnitude of the relaxations, but there still remains the outward displacement. In ionic compounds such as MgO and ZnO, large outward relaxations around a vacancy could be induced by the Coulomb repulsion between atoms surrounding the vacancy.[21,22] However, the origin of outward relaxation around defects in intermetallic compounds has not been reported. We will discuss this in detail below.

IV. ELECTRONIC STRUCTURES

A. Bulk CoAl and CoTi

The site-projected partial density of states (PDOS) for the bulk systems of CoAl and CoTi are shown in Fig. 3. These curves are shifted so as to set the Fermi level at zero. Electronic structure calculations were reported for a series of transition-metal (TM) aluminides[23–26] (FeAl, CoAl, and NiAl) or a series of TM titanides (FeTi, CoTi, and NiTi).[9–11] It was found that the features of the DOS within both series are rather similar and a rigid band shift is roughly applicable for the change in the electronic structure across the series. We will focus on the difference between the CoAl and CoTi since little attention has been given to this point. The features of these DOS curves in this paper agree well with the above-mentioned previous works. The overall shape of the DOS curve of the Co atom is similar for CoAl and CoTi except for the peak intensities. A deep minimum, separating bonding and antibonding states, around the Fermi level appears in CoAl and CoTi, while the position of the deep minimum for CoAl is about 0.4 eV higher in energy than that for CoTi. The Fermi level in CoTi is located at the upper band composed of the antibonding states. This indicates that the antibonding contribution in CoTi is larger than that in CoAl in which the Fermi level falls near the minimum.

For a further understanding of the chemical bonding, the valence electron density and the bonding charge density, which is the difference between the self-consistent electron density and the superposition of atomic electron densities, on the (110) plane are presented in Fig. 4. While the Ti-3p electrons are treated as valence electrons in present calculations, the valence electron-density plots do not include the Ti-3p electrons. The analysis for the bonding mechanism using electron-density plots was performed for TM aluminides by Fu and Yoo,[27] by Zou and Fu,[28] and by Sundararajan *et al.*[25] and for TM titanides by Eibler *et al.*[9] Their results indicate that the formation of the directional bonding is more pronounced in FeAl or in FeTi and the ionic bonding character induced by the charge transfer from Al/Ti to the TM atoms increases with the atomic number of the TM atoms. The change in the bonding character in going from Fe to Ni is a common feature for TM aluminides and TM titanides. However, the difference in the chemical bonding between TM aluminides and TM titanides is still unclear.

In the bonding charge density plot for CoAl, an increase in the electron density of the t_{2g} component of the Co d band, which contributes to the directional Co-Al bonding, is observed accompanying a depletion of electron density of the e_g component. The valence electron-density plot for CoAl shows the anisotropic charge distribution around the Co atoms, which also indicates the formation of the Co-Al bonding. On the other hand, while a depletion of the electron density is also observed around the Co atoms in CoTi, a significant increase of the electron density in the direction of the Co-Ti bonding does not appear. Consequently, a covalent bonding character is more pronounced in CoAl than in CoTi and the opposite trend is observed with respect to an ionic bonding character. The difference in the bonding character also appears in the second nearest bonding. While the electron density of the Co-Co bonds is larger than that of the Ti-Ti bonds in CoTi, the electron densities of the Co-Co and Al-Al bonds in CoAl are comparable, which originates from the large extent of the Al-sp orbitals.

B. Monovacancies

Judging from the bond length in pure metal phases, larger inward relaxations around the Al and Ti vacancy are expected than that around the Co vacancy. However, in CoAl, the relaxation of the nearest-neighbor atoms around the Al vacancy is smaller than that around the Co vacancy. Moreover, in CoTi, the direction of the relaxation of the nearest-neighbor atoms around the Ti vacancy is not inward but outward. In ionic compounds such as MgO and ZnO, the outward relaxation around the vacancy is induced by the

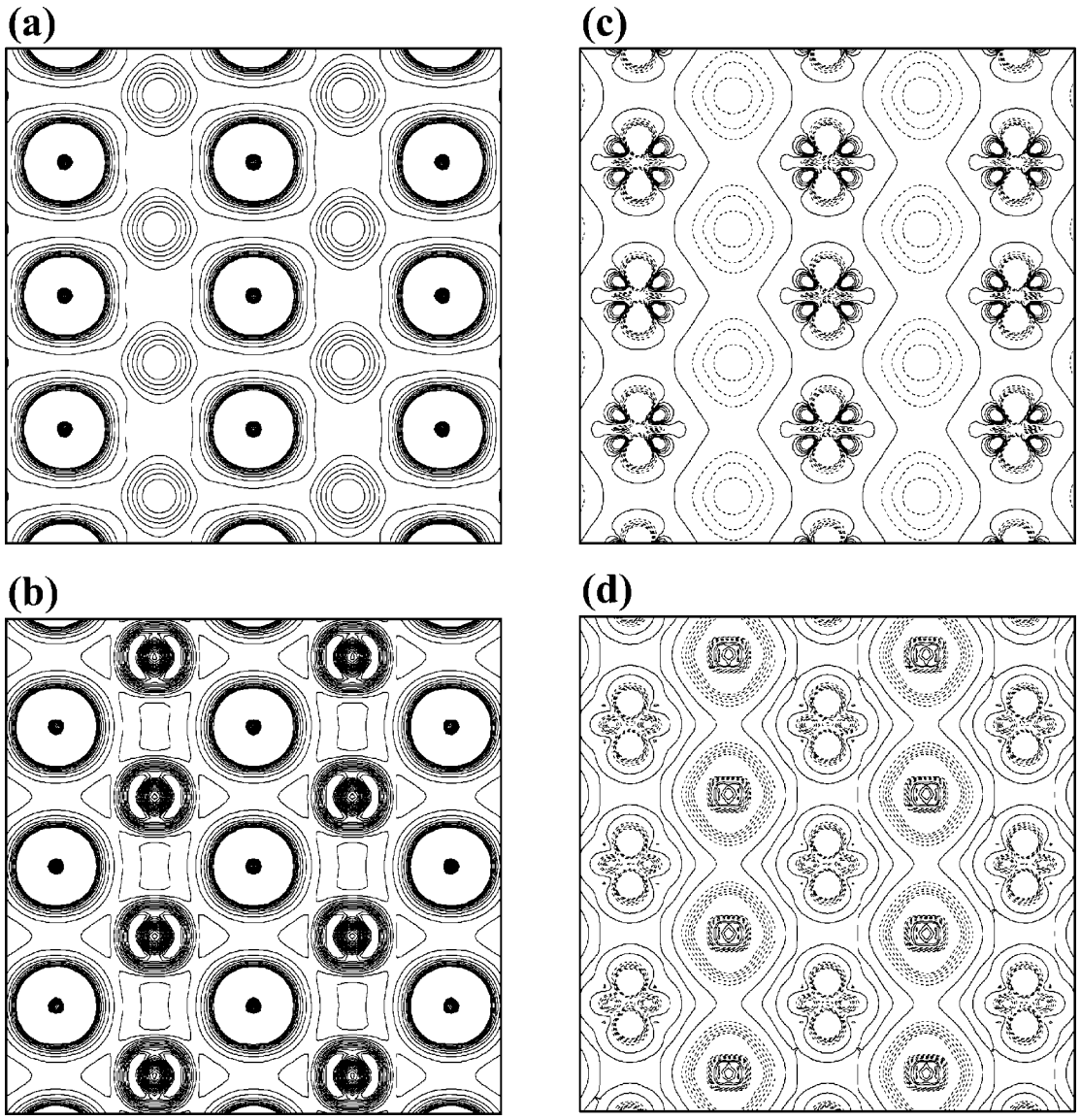

FIG. 4. The valence electron density (upper panels) and the bonding charge density (lower panels) on the (110) plane in CoAl (left panels) and CoTi (right panels). The central position in each panel corresponds to the Co site. The interval of contour lines corresponds to 0.0067 and 0.004 electrons/$Å^3$ in the valence electron-density plots and the bonding charge-density plots, respectively.

Coulomb repulsion between the nearest-neighbor atoms. To the best of our knowledge, the origin of the outward relaxation as seen in CoTi has not been well discussed in intermetallic compounds. In order to elucidate the origin of the outward relaxation around the Ti vacancy, the chemical bondings are examined for the results calculated without structural relaxations. Figures 5 and 6 show contour plots for the valence electron density around the vacancy in the (110) plane in CoAl and CoTi, respectively. Contour plots for the difference in the electron density with and without a vacancy are also presented in the lower panels to observe the change in the electron density induced by the vacancy more clearly.

The electron density of the Co-Ti bonds around the Co vacancy increases by the formation of the Co vacancy. Because the charge transfer occurs from the Ti to Co atoms in CoTi, the formation of Co vacancy induces the excess of electrons around the vacancy. As a result, the excess of electrons is redistributed around the Co vacancy and strengthens the Co-Ti bonds. The charge redistribution around a vacancy occurs in pure metal systems[29] because the bonds broken by the formation of a vacancy supply the excess of electrons. The difference between intermetallic compounds and pure metals is the effective charge induced by the formation of the vacancy. The charge redistribution around the Co vacancy in CoTi arises from not only the breaking of the bonds but also the screening for the effective positive charge of the vacancy site surrounded by the positively charged Ti atoms. The charge redistribution in CoTi is, therefore, more pronounced than that in pure metals. In order to screen the effective positive charge, the decrease in the electron density of the Co-Ti bonds outside the neighboring Co atoms occurs in addition to the increase in the electron density of the Co-Ti

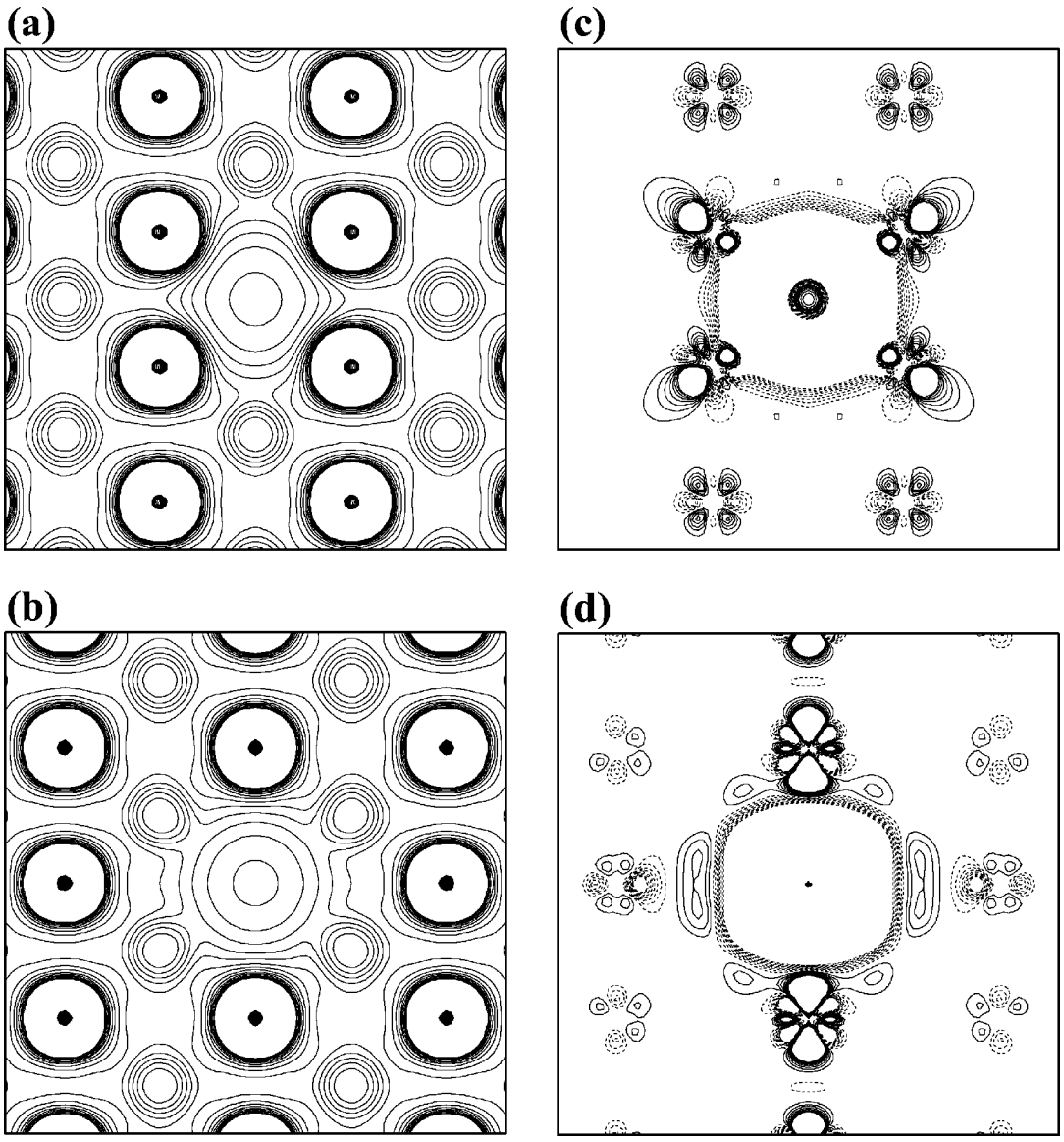

FIG. 5. The valence electron density (upper panels) and the difference in electron density (lower panels) for the Al vacancy (left panels) and the Co vacancy (right panels) on the (110) plane in CoAl. The interval of contour lines corresponds to 0.0067 and 0.0005 electrons/$Å^3$ in the valence electron-density plots and the difference in electron-density plots, respectively.

bonds around the Co vacancy. A similar tendency can be seen around the Co vacancy in CoAl, whereas the increase in the electron density is not as large as in CoTi because the charge transfer from Al to Co in CoAl is smaller than that from Ti to Co in CoTi. However, the Al-Al bonds as well as the Co-Al bonds around the Co vacancy gain the electron density. The compensation for the deviation from the stoichiometry by the Co vacancy in the Al-rich CoAl is, therefore, energetically more favorable than that in CoTi as seen in Fig. 1.

On the other hand, the formation of the Ti vacancy leads to the depletion of electrons around the Ti vacancy. As seen in Fig. 6, the electron density of the bonds between Co and Ti around the Ti vacancy decreases in contrast to the case of the Co vacancy, while the significant increase in the electron density is observed between the neighboring Co atoms and the Ti atom that is located in the counterside of the Ti vacancy. This is due to the charge redistribution for the screening on the effective negative charge of the vacancy site. The Ti vacancy site surrounded by the negatively charged Co atoms has a negative charge. In order to screen the effective negative charge of the vacancy site, the charge redistribution occurs from the inside to the outside of the region surrounded by the neighboring Co atoms and the bonding charge of the Co-Ti bonds outside the neighboring Co atoms increases. As a result, this charge redistribution strengthens these Co-Ti bonds site and leads to the outward relaxation of the Co atoms around the Ti vacancy. The charge redistribution around the Al vacancy in CoAl is not large enough to induce the outward relaxation of the Co atoms because the amount of charge transfer in CoAl is smaller than that in CoTi, as pointed out above. However, the inward relaxation

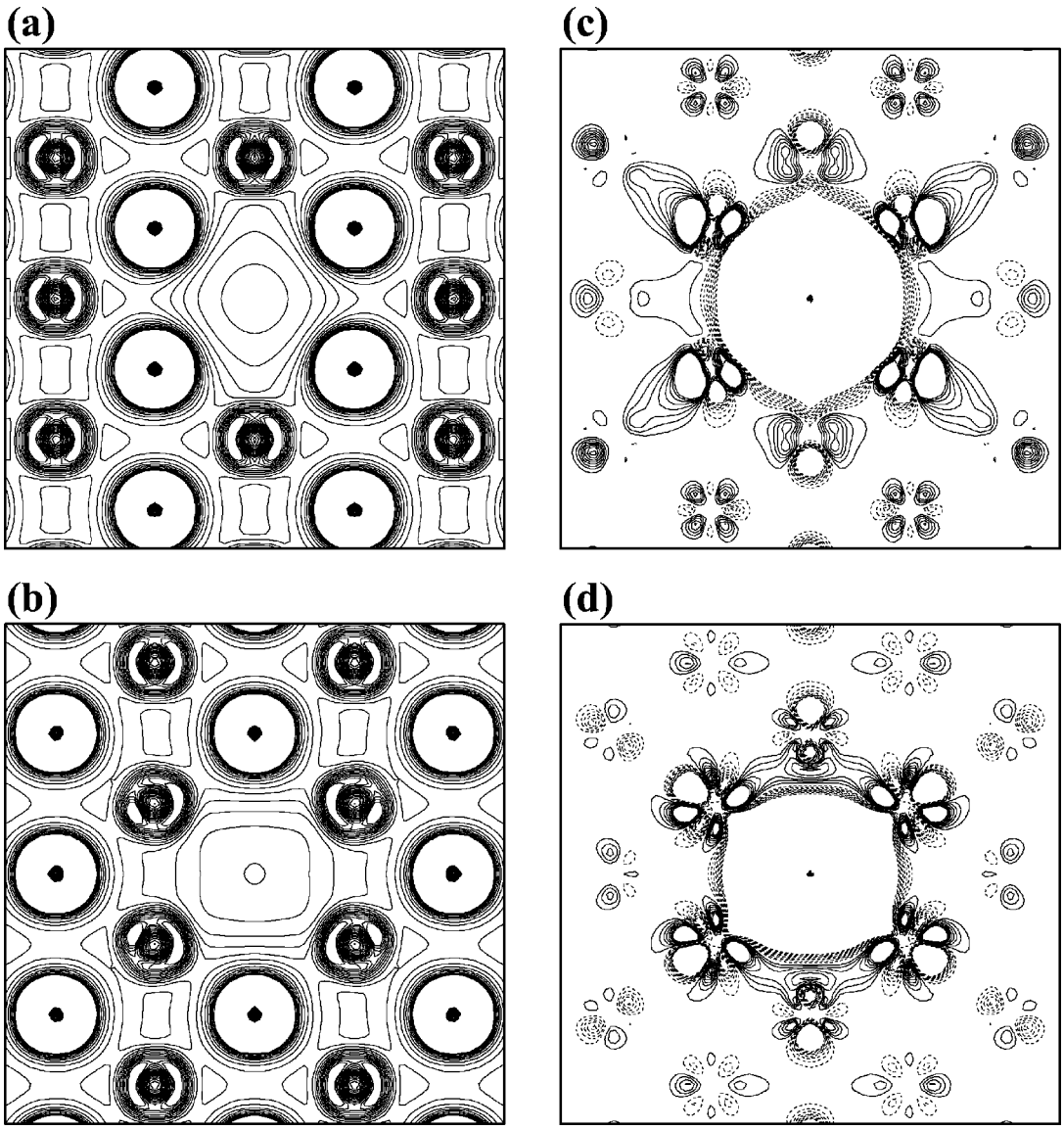

FIG. 6. The valence electron density (upper panels) and the difference in electron density (lower panels) for the Ti vacancy (left panels) and the Co vacancy (right panels) on the (110) plane in CoTi. The interval of contour lines corresponds to 0.0067 and 0.0005 electrons/Å^3 in the valence electron-density plots and the difference in electron-density plots, respectively.

around the Al vacancy is reduced and becomes smaller than that around the Co vacancy against the atomic size difference owing to the charge redistribution.

The formation of a vacancy in MgO also induces the charge redistribution.[21] The charge redistribution is observed in the atoms surrounding the vacancy in order to screen the effective charge. However, the bonding charge is not induced by the formation of vacancies in MgO because there is virtually no covalent bonding between the Mg and the O atom. In ionic compounds such as MgO, the Coulomb repulsion between atoms surrounding the vacancy is responsible for the relaxation around the vacancy. On the other hand, in intermetallic compounds, the ionic bonding character induces the charge redistribution around the vacancy and the covalent bonding character leads to the change in bonding charge density as a result of the charge redistribution.

As seen in Table II, the spin polarization decreases the outward relaxations around the Ti vacancy in CoTi. Figure 7 shows the PDOS of for the neighboring Co atoms around the Ti vacancy in CoTi. The DOS curve of the Co atom in the non-spin-polarized case is very similar to that in bulk CoTi, whereas the spin-polarized calculation yields a magnetic moment. Figure 8 shows contour plots for the valence electron density for the Ti vacancy in CoTi and the difference in the electron density between the spin-polarized and non-spin-polarized calculations without lattice relaxations. The spin polarization of the neighboring Co atoms around the Ti vacancy leads to the filling of the majority Co band, which induces a charge redistribution on the neighboring Co atoms toward the Ti vacancy. As a result, the increase in the bonding electrons around the Ti vacancy strengthens the Co-Co bonding and lowers the formation energy. Although the increase of the Co-Ti bonds outside the Ti vacancy, which induces the outward relaxation, still remains as seen in the valence electron-density plot, the outward relaxation around the Ti vacancy is constrained by the Co-Co bonding.

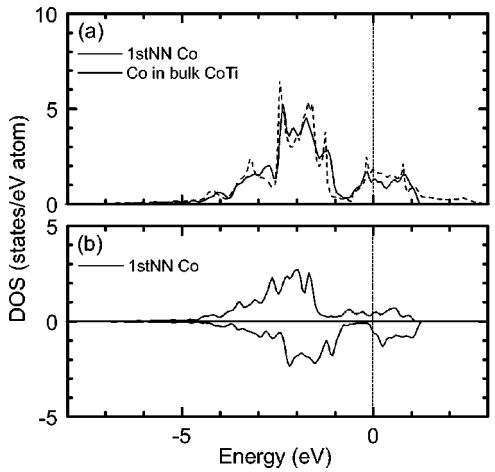

FIG. 7. The site-projected PDOS for the Ti vacancy in CoTi obtained by (a) non-spin-polarized and (b) spin-polarized calculations.

As discussed above, the local charge induced by the vacancy strongly affects the lattice relaxations. This indicates that the positron, which have a positive charge, trapped at a vacancy could affect the lattice relaxations around the vacancy. Positron lifetime measurement allows us to identify the kind of the vacancy trapping a positron because a positron lifetime is inversely proportional to the electron density in which a positron annihilates. The vacancy trapping a positron, therefore, could yield the positron lifetime reflecting the lattice relaxation induced by the trapped positron. In the case of the Ti vacancy in CoTi, the comparison with the measured and theoretical positron lifetimes in the Co-rich CoTi suggests that the inward relaxation occurs around the Ti vacancy in CoTi,[20] which is opposite to the result of this work. However, the positron trapped at the Ti vacancy could reduce the negative effective charge, which induces the outward relaxation, of the Ti vacancy. The possibility of the inward relaxation caused by the positron trapped at the Ti vacancy can be considered. In order to calculate the positron lifetime of vacancies more precisely, the lattice relaxation induced not only by the charge redistribution but also by the trapped positron should be taken into account.

C. Antisite atoms

The formation of the Co antisite atom gives rise to the Co-Co bonding, which can cause a local moment. As seen in Fig. 1, the spin polarization of the Co antisite atom in CoAl depends on the supercell size: the concentration of the Co antisite atom. In order to further examine the dependence, we also performed the calculation using a supercell containing 32 atoms with translation vectors $(0,2a,2a)$, $(2a,0,2a)$, and $(2a,2a,0)$. Figure 9 shows the site-projected PDOS of the Co antisite atom in CoAl calculated using the supercells containing 16, 32, and 54 atoms. The DOS curves for non-spin-polarized and spin-polarized calculations are presented in left panels and right panels, respectively. These curves are shifted so as to set the Fermi level at zero. The general shapes of the three DOS curves for non-spin-polarized calculations are very similar to each other. The DOS of the Co antisite atom in CoAl is clearly split into a bonding state and an antibonding state because of the strong interaction with the neighboring Co atoms. The Fermi level lies slightly above the highest peak in the antibonding region. The DOS of the neighboring Co atoms in CoAl is similar to that in bulk CoAl. However, a difference can be seen in the antibonding band around the Fermi level. The width of the antibonding band decreases linearly with the number of constituent atoms of the supercell. This is because the interaction between the Co antisite atoms diminishes with increasing supercell size. Since the Fermi level lines in the narrow highest peak, the slight change in the shape of the antibonding band appreciably affects the DOS at the Fermi level. The DOS at the Fermi level for the $N=16$ and 32 supercell cal-

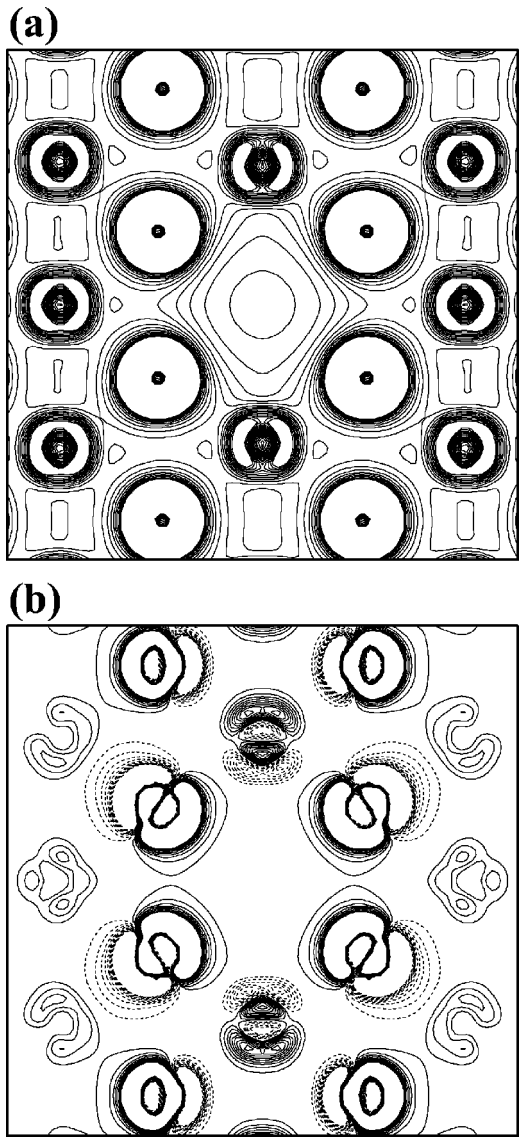

FIG. 8. The valence electron density (a) and the difference in electron density (b) between spin-polarized and non-spin-polarized calculations for the Ti vacancy on the (110) plane in CoTi. The interval of contour lines corresponds to 0.0067 and 0.005 electrons/Å^3 in the valence electron-density plots and the difference in electron-density plots, respectively.

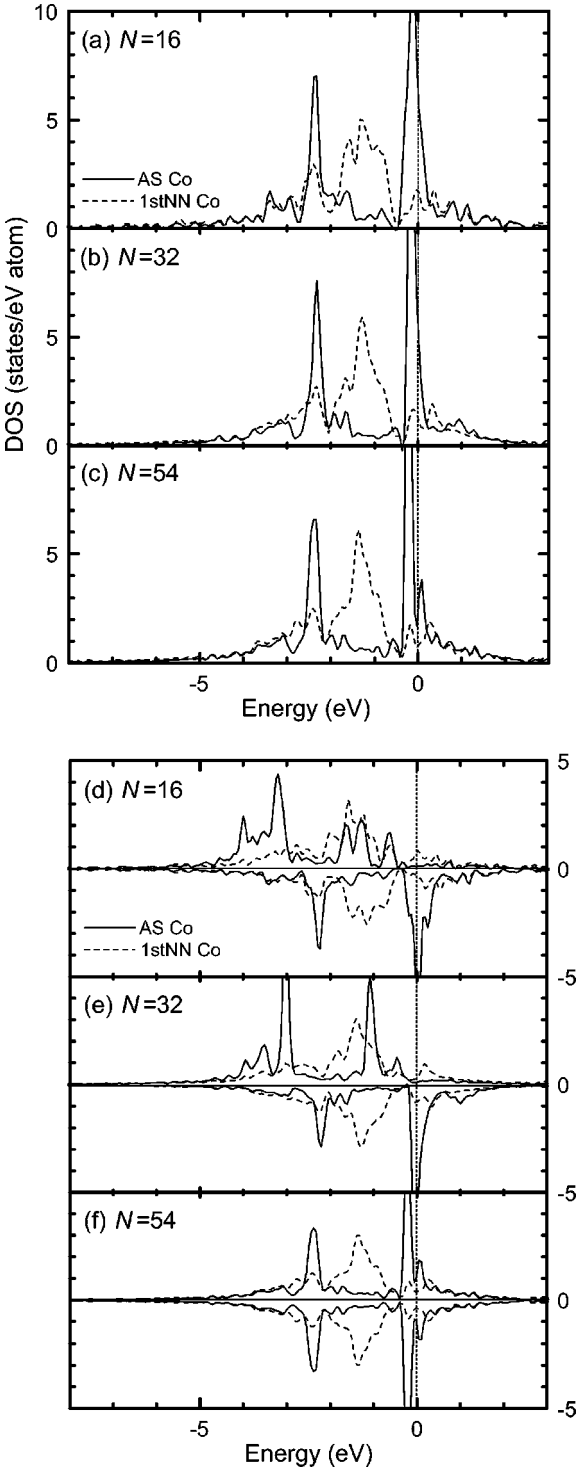

FIG. 9. The site-projected PDOS for the Co antisite atom and its first nearest-neighbor Co atom in CoAl: (a), (b), and (c) PDOS of non-spin-polarized calculation using the $N=16$, 32, and 54 supercell, respectively. (d), (e), and (f) PDOS of spin-polarized calculation using the $N=16$, 32, and 54 supercell, respectively. The majority spin is shown as positive and the minority spin as negative.

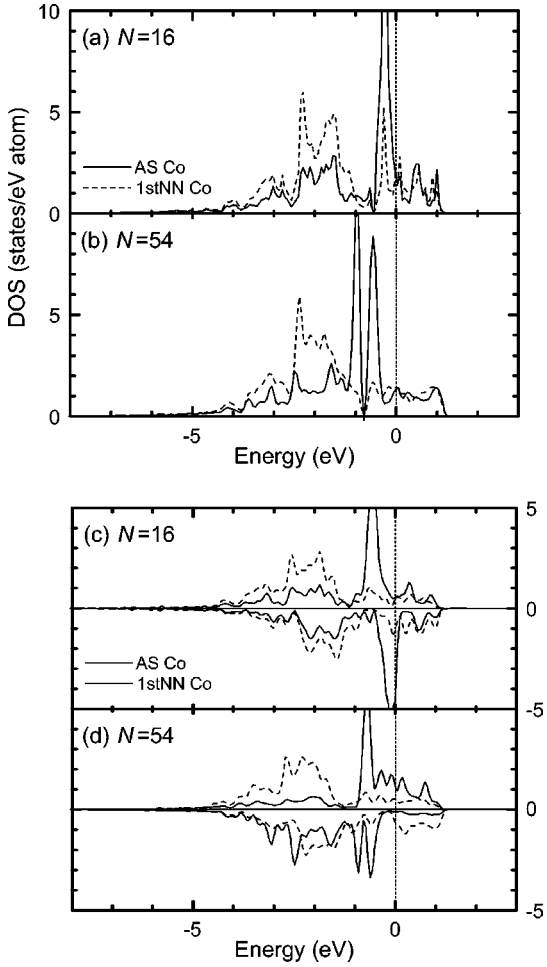

FIG. 10. The site-projected PDOS for the Co antisite atom and its first nearest-neighbor Co atom in CoTi: (a) and (b) PDOS of non-spin-polarized calculation using the $N=16$ and 54 supercell, respectively. (c) and (d) PDOS of spin-polarized calculation using the $N=16$ and 54 supercell, respectively. The majority spin is shown as positive and the minority spin as negative.

culations is much higher than that in bulk CoAl, which induces a local moment of the Co antisite atom. On the other hand, the DOS around the Fermi level for the $N=54$ supercell calculation is split into two bands and the Fermi level is located at a deep minimum separating the two bands. The DOS of the Co antisite atoms for spin-polarized calculations shown in Figs. 9(d)–9(f) reflects the difference of the DOS at the Fermi level in non-spin-polarized calculations: A magnetic moment is induced on the Co antisite atom of the $N=16$ and 32 supercell calculations, whereas the Co antisite atom of the $N=54$ supercell calculation has virtually no magnetic moment. In order to examine the exchange and correlation potentials, we calculated the $N=54$ supercell including a Co antisite atom within the local-density approximation instead of the generalized-gradient approximation. In addition, the calculation of the $N=54$ supercell neglecting the lattice relaxation around the Co antisite atom was also performed. However, there is no significant magnetic moment on the Co antisite atom in the $N=54$ supercell under any conditions employed here. Although there are previous first-principles calculations for the magnetic moment at the Co antisite in CoAl,[5,6] larger supercell calculations than $N=32$ have not been reported. Our magnetic moment of 1.65 μ_B on the Co antisite calculated using the $N=32$ super-

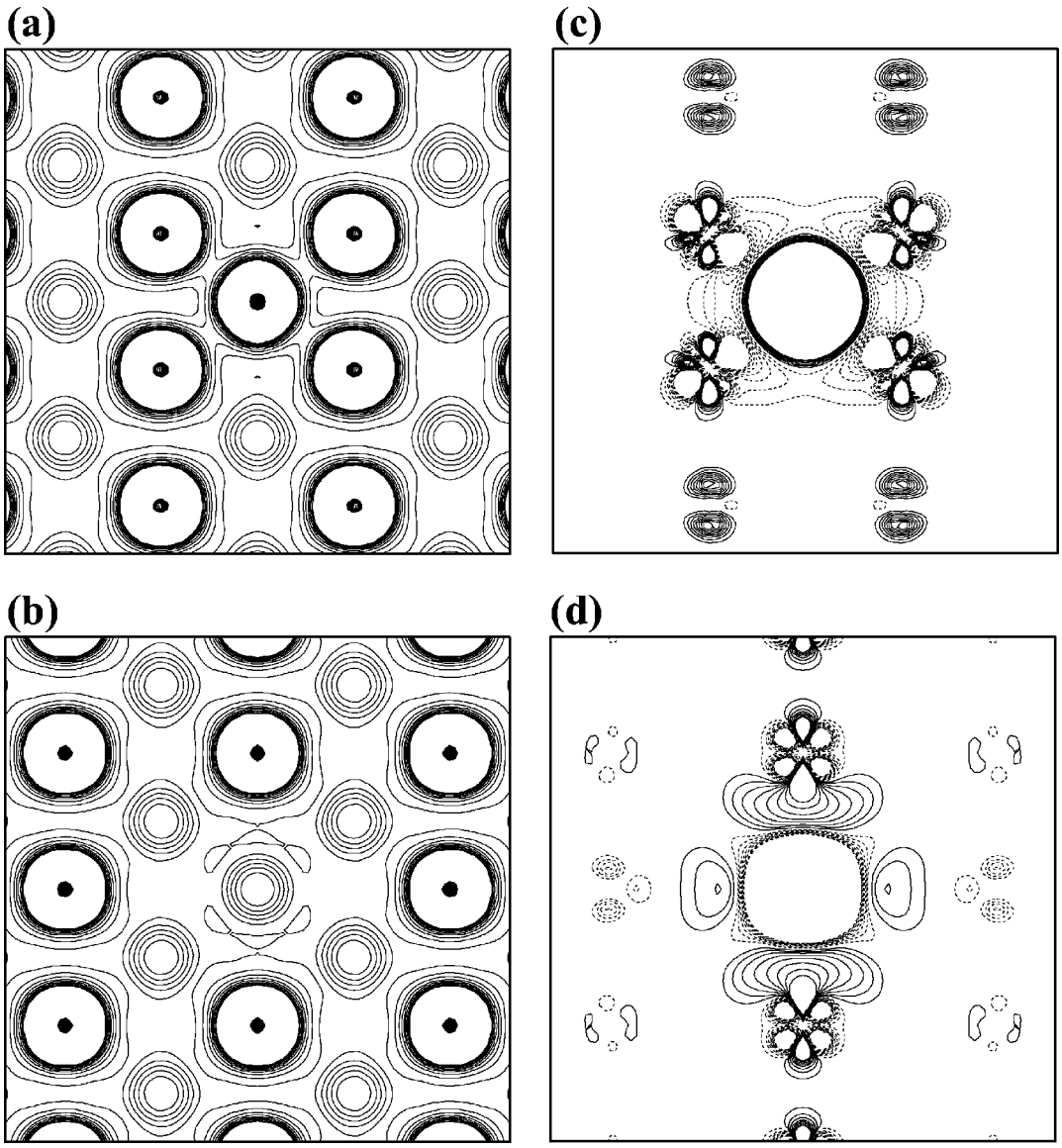

FIG. 11. The valence electron density (upper panels) and the difference in electron density (lower panels) for the Co antisite (left panels) and the Al antisite (right panels) on the (110) plane in CoAl. The interval of contour lines corresponds to 0.0067 and 0.0005 electrons/Å^3 in the valence electron-density plots and the difference in electron-density plots, respectively.

cell is in good agreement with 1.53 μ_B by the recent first-principles calculation with the same size supercell.[5] Our results suggest that the composition of the Co antisite atoms affects the occurrence of a magnetic moment of the Co antisite atoms. There also exist experimental investigations suggesting that a single Co antisite atom carries no moment.[30,31]

Figure 10 shows the site-projected PDOS of the Co antisite atom in CoTi calculated using the supercells containing 16 and 54 atoms. The DOS curves for non-spin-polarized and spin-polarized calculations are presented in left panels and right panels, respectively. In the case of the Co antisite atom in CoTi, there is no sharp peak in the bonding band of Co antisite in CoTi. This reflects the difference in chemical bonding in bulk system: a covalent bonding character is more pronounced in CoAl than in CoTi. Although there is no appreciable change in the DOS of the Co antisite in CoAl for non-spin-polarized calculations with the increase in the supercell size, the antibonding band around the Fermi level for the case of CoTi moves downward and is split into two bands. This is due to the decrease of the Co-Co interaction as a result of the outward relaxation around the Co antisite atom in CoTi as listed in Table III. In order to elucidate the origin of the structural relaxation around the antisite atoms, the valence electron-density plot for the unrelaxed system and the difference in electron density between the antisite and the bulk system in CoAl and CoTi are presented in Figs. 11 and 12, respectively. As discussed in the preceding section, extracting the Ti atom from CoTi brings about the depletion of electrons and negatively charged region around the Ti site. This situation also induces the outward relaxation around the Co antisite atoms in the same manner as the relaxation around the Ti vacancy in CoTi. In the case of the Co antisite, while the existence of the Co atoms at the Ti site reduces these situations, the trends for the charge redistribution

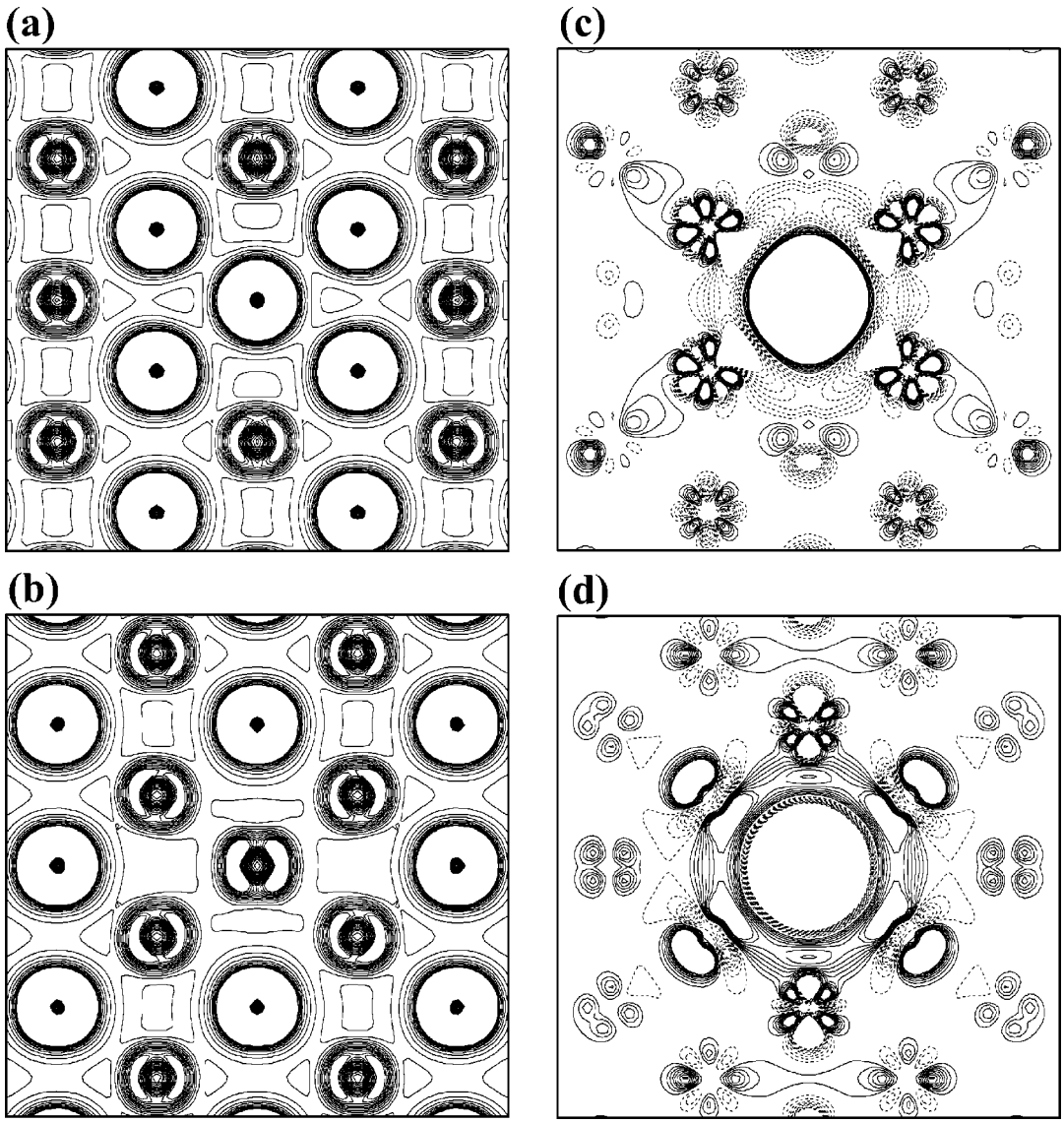

FIG. 12. The valence electron density (upper panels) and the difference in electron density (lower panels) for the Co antisite (left panels) and the Ti antisite (right panels) on the (110) plane in CoTi. The interval of contour lines corresponds to 0.0067 and 0.0005 electrons/Å^3 in the valence electron-density plots and the difference in electron-density plots, respectively.

around the Co antisite atom in CoTi are the same for that around the Ti vacancy in CoTi as seen in Fig. 6: the increase of the electron density between the neighboring Co atoms and the Ti atoms located in the counterside of the Ti vacancy. Therefore, the charge redistribution for screening the effective charge around the Co antisite causes the outward relaxation of the neighboring Co atoms.

In contrast to the case of CoAl, the Co antisite atom in CoTi calculated with the $N=54$ supercell shows a spin polarization. Focusing on energetics, the spin polarizations for both the antisite and the vacancy in the Co-rich side lower the formation energy. As seen in Fig. 2, the energy gains by the spin-polarized calculations for the Co antisite and the Ti vacancy in CoTi are comparable. This indicates that the energy gain mainly arises from the local moments on the neighboring Co atoms around the Ti/Al vacancy or the Co antisite atom. The local moment on the antisite atom hardly contributes to the energy gain because the downward shift of the majority band accompanies the occupation of the antibonding states. This trend can be seen more clearly for the Co antisite atom in CoAl. The spin splits of the neighboring Co atoms around both the Co antisite atom and the Ti vacancy in CoTi are almost of the same value of about 0.5 eV, whereas those around the Co antisite atom in CoAl decrease with the increase of the supercell size: the spin split of 0.44 eV for the $N=16$ supercell calculation becomes smaller and takes the value of 0.11 eV for the $N=32$ supercell calculation. The energy gain by the spin polarization also decreases linearly with the spin split on the neighboring Co atoms.

In the Co-rich side, the Co antisite atom is energetically more favorable than the Co vacancy in both CoAl and CoTi because of the formation of the Co-Co bonds around the Co antisite atom. However, in the Al/Ti-rich side, the situation is more complicated. Regarding the Al/Ti antisite, the Al antisite in CoAl is energetically more costly than the Ti antisite in CoTi as seen in Figs. 1 and 2. Figure 13 shows the bond-

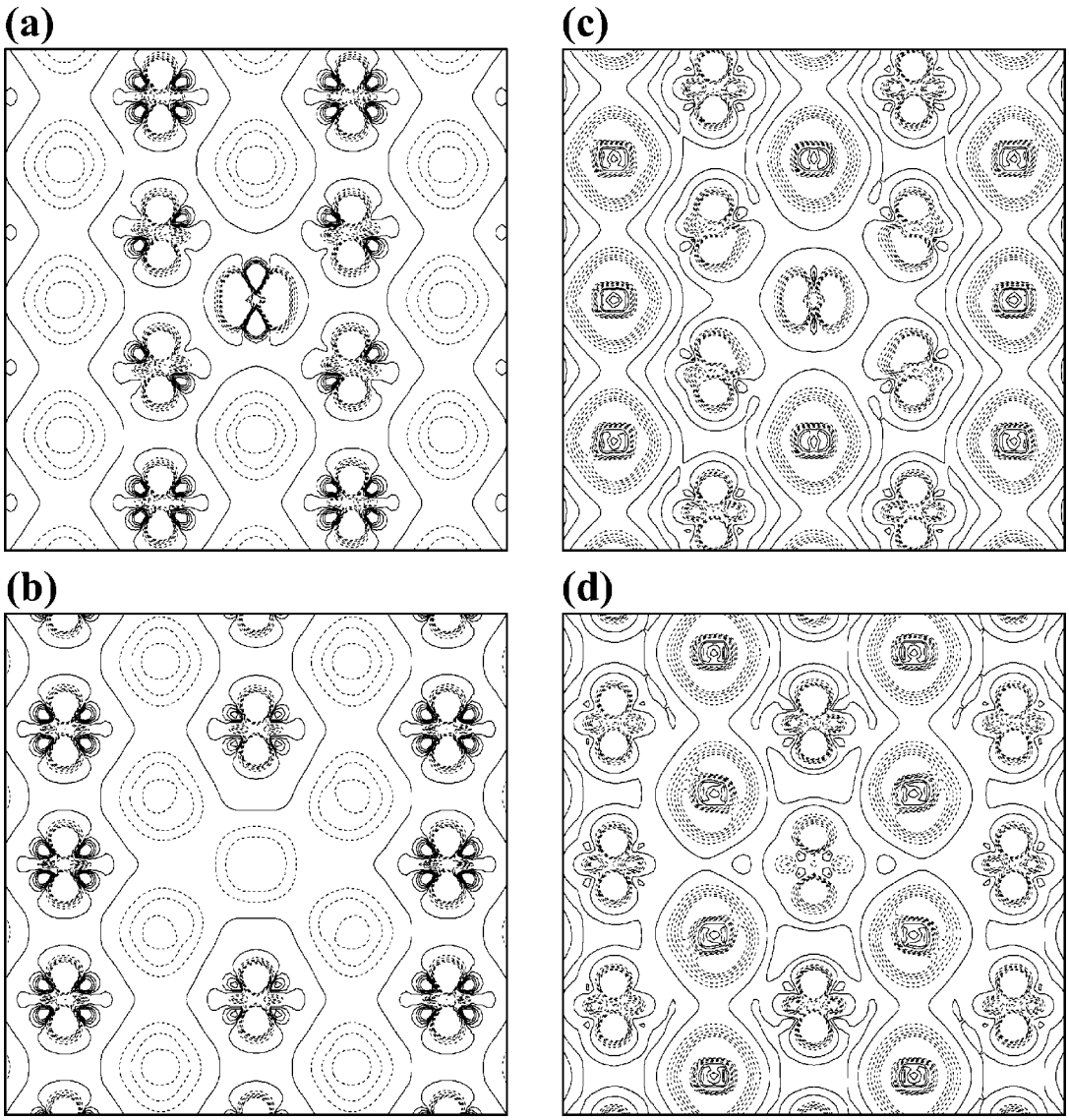

FIG. 13. The bonding charge-density plots on the (110) plane for (a) Co antisite in CoAl, (b) Al antisite in CoAl, (c) Co antisite in CoTi, and (d) Ti antisite in CoTi. The interval of contour lines corresponds to 0.004 electrons/Å^3.

ing charge-density maps for the antisite atoms. While the electron-density distribution around the Ti atom in bulk CoTi is isotropic as seen in Fig. 4, that around the Ti antisite atom shows an increase in the electron density of the t_{2g} component of the Ti-*d* band, indicating the formation of the bonds between the Ti antisite and the neighboring Ti atoms. The situation is similar to not the Ti atom but the Co atom in CoTi. This is because the Ti antisite atom is surrounded by the positively charged Ti atoms and the environment around the Ti antisite atom is similar to the Co atoms. The formation of the Ti-Ti bonds is also observed in the PDOS. Figure 14 shows the PDOS of the Al antisite atom in CoAl and the Ti antisite atom in CoTi calculated using the $N=32$ supercell, respectively. The DOS of the Ti antisite in CoTi has a large peak, which mainly arises from the t_{2g} component of the Ti-*d* band, just below the Fermi level and the unoccupied band just above the Fermi level diminished. This indicates the formation of the bonds between the Ti antisite and the neighboring Ti atoms. In addition, the introduction of the Al/Ti antisite supplies the excess electrons around the antisite atom owing to the charge transfer from the Al/Ti to Co atoms. In the case of the Al antisite atom in FeAl, the excess electrons stabilize the Fe-Al bonds by occupying the unfilled bonding states.[7,8] The bonding states of both the Co-Al and Co-Ti bonds are filled and the charge redistribution to the Co-Al and Co-Ti bonds has a small contribution to the stability. However, the excess electrons around the Ti antisite atom contribute to the stability of the bonds whose bonding states are not filled: the bonds between the neighboring Ti atoms and between the Ti antisite atom and the next-nearest-neighbor Co atoms along [001]. On the other hand, there is no buildup of electron density between the Al antisite and the neighboring Al atoms in CoAl, which indicates that the interatomic distance around the Al antisite atom is not large enough for the Al-Al bonds to be formed. Moreover, the excess electrons around the Al antisite atom in CoAl are not

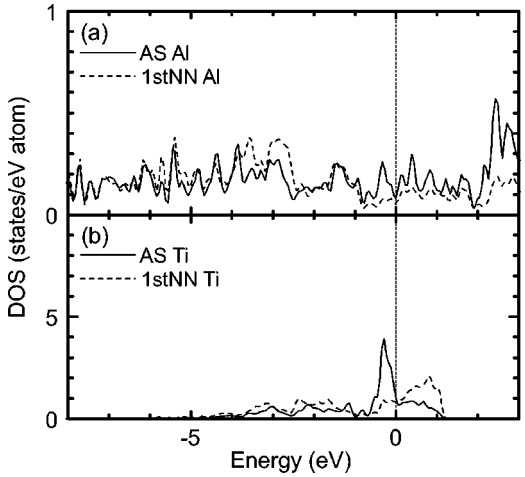

FIG. 14. The site-projected PDOS for the Al antisite in CoAl (a) and for the Ti antisite in CoTi.

so pronounced as that around the Ti antisite atom in CoTi. The introduction of the Al antisite atom in CoAl is, therefore, energetically more costly than that of the Ti antisite atom in CoTi.

V. CONCLUSION

In this paper, we have performed first-principles electronic structure calculations for the constitutional defects in CoAl and CoTi in order to investigate the energetics and structural relaxations. The difference in the bonding character induces the difference in the energetics and structural relaxations for the defects between CoAl and CoTi: a covalent bonding character is more pronounced in CoAl than in CoTi and CoTi has a larger ionic bonding character than CoAl. With respect to the energetics of the defects, the difference between CoAl and CoTi can be seen in the Al/Ti-rich side. The Co vacancy in CoAl is energetically favorable because of the charge redistribution to the Al-Al bonds as well as Co-Al bonds around the Co vacancy. The charge redistribution by the formation of the Co vacancy in CoTi mainly occurs to the Co-Ti bonds around the Co vacancy in order to screen the effective positive charge induced by the Co vacancy. The Ti antisite atom is preferred in the Ti-rich CoTi because of not only the formation of the Ti-Ti bonds but also the increase in the electron density of the Ti-Co bonds and Co-Co bonds around the Ti antisite atoms. The Ti-*d* orbital plays an important role in the formation of the Ti-Ti bonds. The Ti-*d* orbital at the antisite shows the anisotropic character and the t_{2g} component contributes to the Ti-Ti bonding. On the other hand, the interatomic distance around the Al antisite atom in CoAl is not large enough for the Al-Al bonds to form.

The lattice relaxations around the defects are pronounced in CoTi. The large outward relaxations around the Ti vacancy or Co antisite arise from the increase in the electron density of the Co-Ti bonds outside the defect region. This charge redistribution occurs to screen the effective negative charge induced by the Ti vacancy or Co antisite, which originates from the ionic bonding. The mixture of the covalent bonding and ionic bonding leads to the lattice relaxation against the atomic size difference. The atomic size difference is more responsible for the lattice relaxations in CoAl because the charge transfer from Al to Co in CoAl is smaller than that from Ti to Co in CoTi.

The Co-Co bonds around the defects could give rise to the local moment. The spin polarization of the neighboring Co atoms around the Co vacancy or Co antisite contributes to the lower of the formation energy. The Co antisite in CoTi shows the spin polarization irrespective of the supercell size, whereas the spin polarization of the Co antisite in CoAl depends on the supercell size.

Systematic calculations across the periodic table are helpful for further understanding of the defects in intermetallic compounds. Some systematic calculations are currently in progress and will be reported in future.

ACKNOWLEDGMENTS

This work was supported by a Grant-in-Aid for Scientific Research from the Ministry of Education, Culture, Sports, Science and Technology of Japan. This work was partly carried out at the Strategic Research Base ''Handai Frontier Research Center'' supported by the Japanese Government's Special Coordination Fund for Promoting Science and Technology.

*Email address: mizuno@mat.eng.osaka-u.ac.jp

[1] C.L. Fu, Y.Y. Ye, M.H. Yoo, and K.M. Ho, Phys. Rev. B **48**, 6712 (1993).
[2] J. Mayer, C. Elässer, and M. Fähnle, Phys. Status Solidi B **191**, 283 (1995).
[3] G. Bester, B. Meyer, and M. Fähnle, Phys. Rev. B **60**, 14 492 (1999).
[4] B. Meyer and M. Fähnle, Phys. Rev. B **59**, 6072 (1999).
[5] N.I. Kulikov, A.V. Postnikov, G. Borstel, and J. Braun, Phys. Rev. B **59**, 6824 (1999).
[6] N. Stefanou, R. Zeller, and p.H. Dederichs, Phys. Rev. B **35**, 2705 (1987).
[7] C.L. Fu, Phys. Rev. B **52**, 3151 (1995).
[8] N. Börnsen, G. Bester, B. Meyer, and M. Fähnle, J. Alloys Compd. **308**, 1 (2000).
[9] R. Eibler, J. Redinger, and A. Neckel, J. Phys. F: Met. Phys. **17**, 1533 (1987).
[10] J.M. Zhang and G.Y. Guo, J. Phys.: Condens. Matter **7**, 6001 (1995).
[11] D. Cheng, S. Zhao, S. Wang, and H. Ye, Philos. Mag. A **81**, 1625 (2001).
[12] S. Mäkinen and M.J. Puska, Phys. Rev. B **40**, 12 523 (1989).
[13] G. Kresse and J. Hafner, Phys. Rev. B **47**, 558 (1993).
[14] G. Kresse and J. Hafner, Phys. Rev. B **49**, 14 251 (1994).
[15] G. Kresse and J. Furthmüller, Comput. Mater. Sci. **6**, 15 (1996).
[16] G. Kresse and J. Furthmüller, Phys. Rev. B **54**, 11 169 (1996).
[17] J.P. Perdew and Y. Wang, Phys. Rev. B **45**, 13 244 (1992).
[18] S.R. Butler, J.E. Hanlon, and R.J. Wasilewski, J. Phys. Chem. Solids **30**, 1929 (1969).
[19] Y. Aoki, T. Nakamichi, and M. Yamamoto, J. Phys. Soc. Jpn. **27**,

257 (1969).
[20] M. Mizuno, H. Araki, and Y. Shirai, Mater. Trans., JIM **43**, 1451 (2002).
[21] A. De Vita, M.J. Gillan, J.S. Lin, M.C. Payne, I. Štich, and L.J. Clarke, Phys. Rev. B **46**, 12 964 (1992).
[22] A.F. Kohan, G. Ceder, D. Morgan, and Chris G. Van de Walle, Phys. Rev. B **61**, 15 019 (2000).
[23] J.M. Koch and C. Koenig, Philos. Mag. B **54**, 177 (1986).
[24] K. Schlemper and L.K. Thomas, Phys. Rev. B **50**, 17 802 (1994).
[25] V. Sundararajan, B.R. Sahu, D.G. Kanhere, P.V. Panat, and G.P. Das, J. Phys.: Condens. Matter **7**, 6019 (1995).
[26] G.A. Botton, G.Y. Guo, W.M. Temmerman, and C.J. Humphreys, Phys. Rev. B **54**, 1682 (1996).
[27] C.L. Fu and M.H. Yoo, Acta Metall. Mater. **40**, 703 (1992).
[28] J. Zou and C.L. Fu, Phys. Rev. B **51**, 2115 (1995).
[29] K. Carling, G. Wahnström, T.R. Mattsson, A.E. Mattsson, N. Sandberg, and G. Grimvall, Phys. Rev. Lett. **85**, 3862 (2000).
[30] A. Amamou and F. Gautier, J. Phys. F: Met. Phys. **4**, 563 (1974).
[31] D.J. Sellmyer and R. Kaplow, Phys. Lett. **36A**, 349 (1971).